Journal of ELECTRONIC MATERIALS, Vol. 40, No. 6, 2011
DOI: 10.1007/s11664-011-1594-0

Silver Nanoparticle Paste for Low-Temperature Bonding of Copper

HANI ALARIFI,[1,2] ANMING HU,[1,3] MUSTAFA YAVUZ,[1] and Y. NORMAN ZHOU[1]

1.—Department of Mechanical and Mechatronics Engineering, Centre for Advanced Materials Joining, University of Waterloo, 200 University Avenue West, Waterloo, ON N2L 3G1, Canada. 2.—e-mail: halarifi@uwaterloo.ca. 3.—e-mail: a2hu@uwaterloo.ca

Silver nanoparticle (NP) paste was fabricated and used to bond copper wire to copper foil at low temperatures down to 160°C. The silver NP paste was developed by increasing the concentration of 50 nm silver NP sol from 0.001 vol.% to 0.1 vol.% by centrifugation. The 0.001 vol.% silver NP sol was fabricated in water by reducing silver nitrate ($AgNO_3$) using sodium citrate dihydrate ($Na_3C_6H_5O_7{\cdot}2H_2O$). The bond was formed by solid-state sintering among the individual silver NPs and solid-state bonding of these silver NPs onto both copper wire and foil. Metallurgical bonds between silver NPs and copper were confirmed by transmission electron microscopy (TEM). The silver NPs were coated with an organic shell to prevent sintering at room temperature (RT). It was found that the organic shell decomposed at 160°C, the lowest temperature at which a bond could be formed. Shear tests showed that the joint strength increased as the bonding temperature increased, due to enhanced sintering of silver NPs at higher temperatures. Unlike low-temperature soldering techniques, bonds formed by our method have been proved to withstand temperatures above the bonding temperature.

Key words: Ag nanoparticles, sintering, wire bonding

INTRODUCTION

Developing a bonding method that can work at temperatures below 250°C is important for the development of polymer-based flexible electronics.[1] It is also economically effective to decrease the bonding temperatures for electronic packaging and interconnections. On the other hand, it is desirable that these joints can bear high-temperature environments such as in electronic circuits near car engines. Thus, forming joints that can withstand higher temperatures than the bonding temperature has great advantage over soldering techniques, which form bonds that cannot withstand high temperatures due to the low melting point of the soldering material.[2]

It has been shown that it is possible to bond two pieces of copper through a sintered network of silver nanoparticles (NPs).[3,4] These bonds are formed by sintering of individual silver NPs combined with sintering of these NPs onto copper surfaces. The sinterability between individual silver NPs and the sinterability of the NPs onto the copper surface determine the strength of the bond. Sintering of NPs occurs at temperatures much lower than that of microparticles due to their high surface-to-volume ratio.[5] Silver NPs were observed to sinter at a temperature as low as 150°C in ambient air.[6] Sintering of silver NPs on a copper substrate was observed at 100°C by *in situ* ultrahigh-vacuum transmission electron microscopy (TEM).[7]

The decrease of the sintering temperature is due to the large driving force of sintering and the high coefficient of diffusion at the nanoscale. In principle, the driving force of sintering can be estimated by the formula $\sigma \approx \gamma\kappa$, where γ is the specific surface energy and κ is the curvature of the surface. It has been shown that the specific surface energy of NPs is significantly higher than that of the bulk.[8] The curvature of the surface is equal to $(1/R_1 + 1/R_2)$, where R_1 and R_2 are the principal radii of

(Received December 22, 2009; accepted February 10, 2011; published online March 1, 2011)

curvature. Thus, the driving force of sintering is inversely proportional to the size of the particles.

On the other hand, the activation energy of diffusion decreases as the size of the nanocrystals decreases.[9] Thus, the corresponding coefficient of diffusion increases based on the Arrhenius equation. The increase of the coefficient of diffusion of the NPs leads to higher sintering rates than that of microparticles. At the early stage of heating, two particles form an initial point contact and surface diffusion starts, which results in the formation of a neck and a grain boundary between the two particles. At later stages of heating, neck growth continues and grain boundary diffusion occurs. After a long enough time, the two particles coalesce and form one larger particle.[10]

Silver NPs coated with organic shells have been used to bond metals at temperature as low as 250°C.[11–14] These bonds were formed by sintering of NPs, which started at the temperature at which the organic shell decomposes. Very recent studies have shown that sintering of NPs can occur at room temperature (RT) by removing the dispersant using methanol.[15,16] However, the method of using methanol to remove dispersant has not been applied for bonding of metals.

Our recent work confirmed that a sintered network of silver NPs can work as a bonding structure for copper wires at 160°C.[17] The used silver NPs are coated with a 1-nm- to 3-nm-thick organic shell of citrate groups. The thickness of the organic shell was determined by high-resolution TEM.[17] This organic shell prevented sintering of silver NPs at RT. The concentration of NPs in water was increased by centrifugation to enable us to develop silver NP paste with concentration of 0.1 M. Metallic bonds between silver NPs and copper pellets was confirmed at bonding temperatures of 250°C and 300°C.

The main goal of this research is to develop a simple low-cost technique to bond copper wires at very low temperatures, and to investigate the effect of bonding temperature on bond strength. The microstructure of the interface between silver and copper wire was examined by scanning electron microscopy (SEM) and TEM. Moreover, the decomposition temperature of the organic shell and its role in promoting the bonding are discussed. The bond strength was investigated at a higher temperature than the temperature at which the bond was formed. The effects of temperature and time on the sintering behavior of the bonding paste were examined by SEM.

EXPERIMENTAL PROCEDURES

Copper Foils and Wires

The copper foils received from the manufacturer were of 50 μm thickness and 5 cm width (McMaster Carr, Aurora, OH). The foils were cut across their length into 5-cm pieces using a shear cutter. The used copper wires were of three different diameters: 50 μm, 250 μm, and 500 μm (McMaster Carr, Aurora, OH). The wires were cut into 10-cm pieces. Prior to bonding, the foils and the wires were ultrasonically cleaned in acetone for 3 min and rinsed by ultrapure water (electrical resistivity approximately 16 MΩ cm to 18 MΩ cm).

Fabrication of Silver NPs Sol

Reduction of metal ions by reducing agents is a common way to fabricate metallic NPs.[18] In this work, silver NPs were prepared by the reduction action of silver nitrate ($AgNO_3$) using sodium citrate dihydrate ($Na_3C_6H_5O_7{\cdot}2H_2O$).[19,20] A solution of ($AgNO_3$, 1 mM) in 250 mL ultrapure water was heated to 80°C. A volume of 10 mL aqueous solution of ($Na_3C_6H_5O_7{\cdot}2H_2O$, 0.34 mM) was then added to the $AgNO_3$ solution. Heating was continued to 90°C for 30 min after adding the citrate solution. The color of the solution changed from the colorless water to yellow after 15 min of heating, and to gray after 25 min. The produced sol is simply silver NPs coated with organic shell and dispersed in water with a concentration of 0.001 vol.%. The excess amount of citrate used in this reaction is responsible for coating the NPs with a 1-nm to 3-nm organic shell. The thickness of the organic shell was confirmed by previous TEM examination of the NPs.[17]

The fabricated silver NPs had an average size of 50 nm and size distribution in the range of 20 nm to 100 nm. A few silver nanobars were found in the prepared sol as a result of different growth rates at different crystallographic planes of the particles. The length of the nanobars was approximately 100 nm, and their diameter ranged from 10 nm to 20 nm. The amount of nanobars might be reduced by adding aniline to the $AgNO_3$ solution prior to heating.[21] However, precise control of the shape and the amount of the nanobars is beyond the scope of this paper.

Fabrication of Silver NPs Paste

The silver NP paste was simply fabricated by increasing the concentration of the silver NP sol from 0.001 vol.% to 0.1 vol.% by centrifugation. A centrifugal force of $1700 \times g$ was applied for 30 min on 15-mL centrifuge tubes (length 118.54 mm, outer diameter 15.62 mm) filled with 0.001 vol.% sol. As a result of the centrifugal force, the silver NPs condensed at the bottom of the centrifuge tubes, leaving only water on top. The water was extracted from the centrifuge tubes using a pipette, leaving 0.15 mL 0.1% silver NP sol (silver NP paste) at the bottom. The carrier of the silver NP paste was just water. This paste was used for all experiments in this work.

Deposition Control of Silver NPs Paste

A fine needle attached to a 10-mL syringe was used to extract the silver NP paste from the

centrifuge tubes and deposit it onto the copper foils. After depositing one droplet of paste onto the copper foil, the silver NPs migrated to the edge of the droplet, showing the coffee-ring effect (CRE).[22] This resulted in an undesirable variation in the thickness of the deposited layer. Thus, to suppress CRE, multiple depositions of the paste on copper foil were performed. This led to relatively uniform thickness within the droplet. A volume of 0.15 mL of the silver NP paste was deposited on each bonded sample. The number of depositions per sample was in the range of 22–30 droplets. This gave a droplet volume of approximately 0.006 mL and approximately 97 μg silver NPs for each deposition. The droplets were dried at 80°C after each deposition.

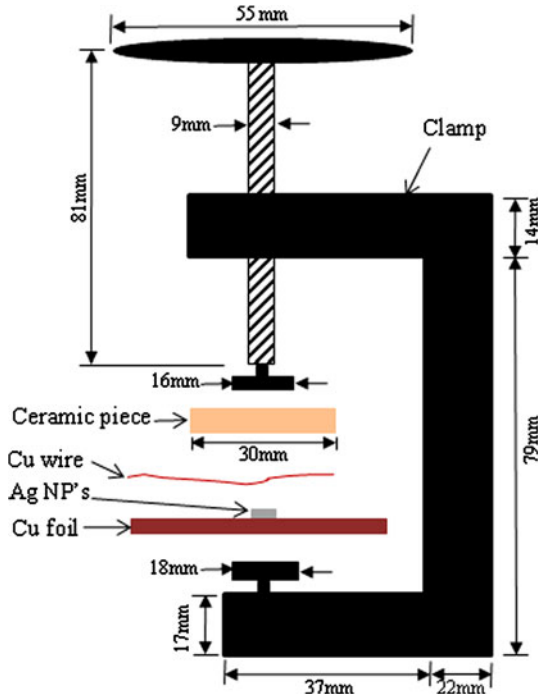

Fig. 1. Schematic diagram of clamping the copper wire to the foil.

Bonding Technique

After depositing the silver NPs onto the copper foil, the copper wire was mounted on the silver NP paste and clamped by a 2-inch screw clamp. A schematic diagram of the clamping geometry is shown in Fig. 1. An alumina ceramic piece was placed underneath the screw to prevent bonding between the silver NPs and the metallic screw. The pressure exerted on the sample was 5 MPa, which was determined by dividing the applied force by the area of the ceramic piece. The applied force was measured using a load cell. A torque wrench was used to tighten the screw and thus to exert the same force on all samples. The clamped sample was then heated at the bonding temperature for 30 min.

Shear Testing

Shear testing was applied by shearing the wire at a rate of 5 mm/min. Figure 2a shows an optical image of a 50-μm copper wire bonded to silver NPs, and a schematic diagram of the shear test is shown in Fig. 2b. To avoid bending on the joint, the wire was clamped at a distance of 7 cm from the joint. The maximum shear strength was calculated by dividing the maximum force by the area of the bond. Three samples were tested for each shear experiment.

The used needle deposited droplets that covered the foil with a circular area of 4.00 ± 0.25 mm in diameter; any extra area resulting from uncontrolled deposition was scratched. After clamping, the copper wire deformed to a nearly elliptical shape and formed a contact with the silver NPs. The contact area was estimated by multiplying the length of the cross-sectional contact between the deformed wire and the foil by the diameter of the silver NP coverage on the foil. Both lengths were measured for each sample by optical microscopy.

Shear testing at high temperature was performed by heating the unbonded side of the foil using a heat gun. The temperature of the sample was measured using a thermocouple attached to the bonded side, 10 mm away from the joint. The shear test was run just after the joint reached the desired temperature.

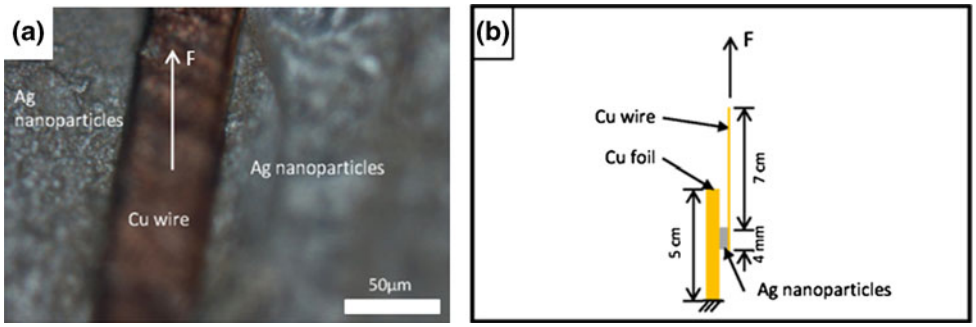

Fig. 2. (a) Optical image and (b) schematic diagram of a shear sample.

Microstructure Analysis

A field-emission scanning electron microscope (Leo1530 FE-SEM; Zeiss, Germany) was used to study the microstructure of the sintered NPs and the bonded samples. The sintering studies were performed by depositing one droplet of the silver NP paste on silicon wafers. The sintering measurement was based on measuring the neck size of the sintered NPs. The neck size was defined as the diameter of the neck that formed between two NPs as they joined together. ImageJ software was used to measure the neck size from SEM images. The sizes of at least 10 necks per sample were averaged.

The bonded samples were mounted in epoxy, cross-sectioned, and then polished by 0.25-μm diamond paste. The samples were coated with a 10 nm gold layer prior to SEM observation. For TEM studies, the bonded samples were sectioned by microtomy.

Thermogravimetric Analysis (TGA) and Raman Spectroscopy

TGA was performed by heating the silver NP paste from RT to 450°C. To study the effect of annealing of the silver NP paste on the decomposition of the organic shell, the paste was annealed at 160°C and 200°C for 30 min prior to the TGA tests. The tests were run in air with a heating rate of 5°C/min.

Raman spectroscopy of the silver NPs was performed to identify the composition of the organic shell and to study the effect of annealing of the silver NP paste on the decomposition of the organic shell. The Raman spectra were recorded using a Renishaw spectrometer excited with an Ar laser at wavelength of 488 nm. The samples were prepared by depositing silver NP paste on a silicon wafer.

RESULTS AND DISCUSSION

Organic Shell Decomposition and Sintering of Silver NPs

Figure 3 shows that the concentration of silver NPs was dramatically increased after centrifugation. TGA analysis of the silver NPs is shown in Fig. 4. The percentage weight loss showed two major drops in sample weight. The first, at 100°C, corresponds to evaporation of water. The second weight loss, between 150°C and 200°C, corresponds to decomposition of the organic shell. These weight drops disappeared after annealing the NPs for 30 min at 160°C and 200°C. This indicates that most part of the organic shell was decomposed at these temperatures.

Raman spectroscopy analysis of the silver NPs annealed at 200°C for different times is shown in Fig. 5. The resulting Raman peaks correspond to CH_2 at 2919 cm^{-1} (2939 cm^{-1}),[23] COO group and CO_3 at 690 cm^{-1} (663 cm^{-1} to 683 cm^{-1}),[23] 1375 cm^{-1} (1360 cm^{-1} to 1373 cm^{-1}),[23] and 1522 cm^{-1} (1470 cm^{-1} to 1530 cm^{-1}),[23] $AgCO_3$ at 1056 cm^{-1} (1072 cm^{-1}),[24] and CO at 2116 cm^{-1} (2143 cm^{-1}).[24] The intensities of the hydrocarbon peaks decreased as the annealing time increased due to the continuous decomposition of the organic shell. The Raman curve for 5 min of annealing showed very weak hydrocarbon peaks, which confirms the decomposition of the organic shell.

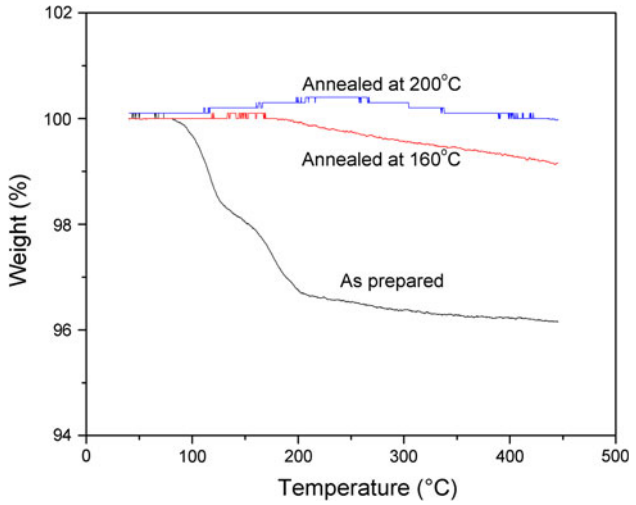

Fig. 4. TGA curves of silver NPs sintered at RT, 160°C, and 200°C.

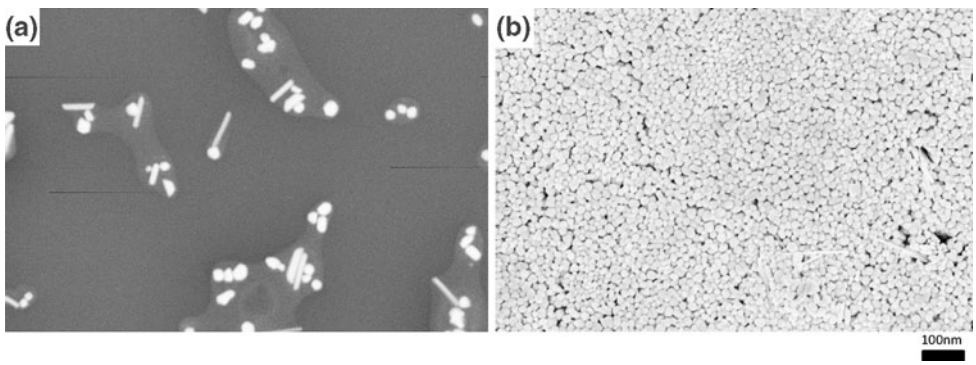

Fig. 3. Concentration of silver NPs (a) before and (b) after centrifugation.

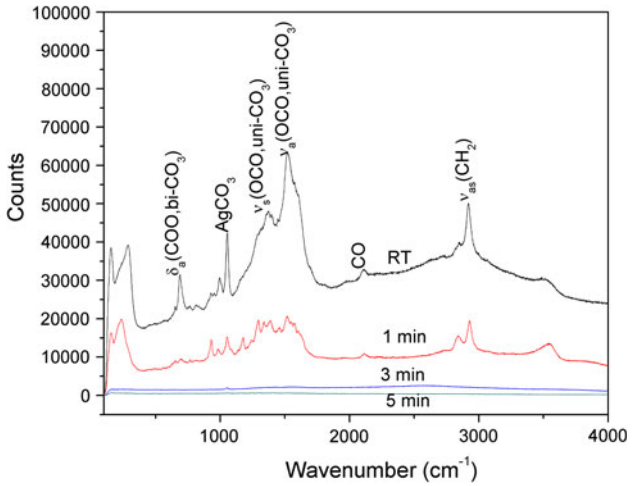

Fig. 5. Raman spectroscopy of silver NPs annealed at 200°C for different times.

Figure 6 shows the effect of sintering time at 200°C on the pressureless sintering behavior of silver NPs. The degree of sintering was enhanced as the period of sintering increased. Measurement of the sizes of a few necks and grains is shown in the figure. The relationship between the sintering time and the neck size is shown in Fig. 7. Neck growth was observed after 1 min of sintering, it continued for 5 min, and then the neck size became nearly constant. With molecular dynamics (MD) simulation, Ding et al.[25] predicted that the neck size grows very quickly at the initial stage of sintering, and then gradually saturates. The present work confirms these theoretical results.

The effect of sintering temperature on the sintering behavior of silver NPs is shown in Fig. 8. The silver NPs were sintered for 30 min at 100°C, 150°C, 200°C, 250°C, and 300°C. The SEM images

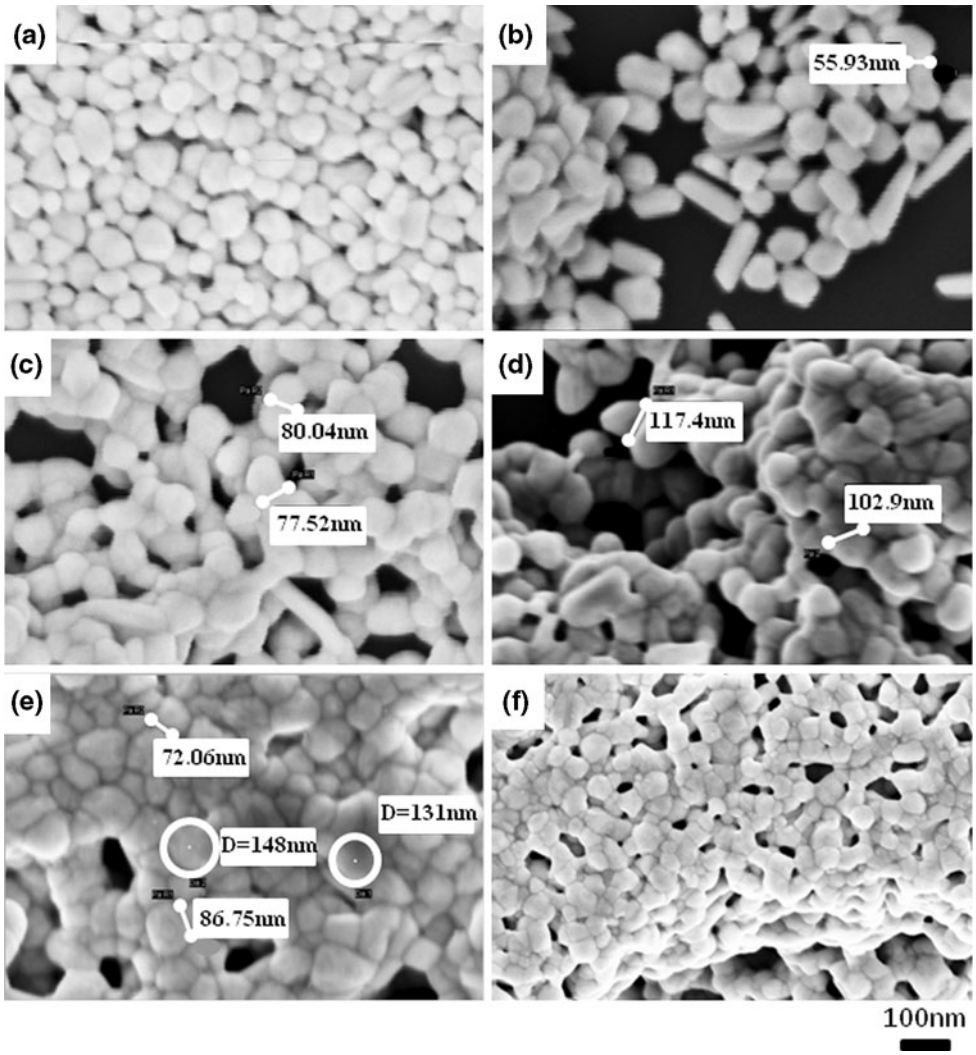

Fig. 6. SEM images of silver NPs (a) at RT and sintered at 200°C for (b) 1 min, (c) 3 min, (d) 5 min, (e) 10 min, and (f) 30 min.

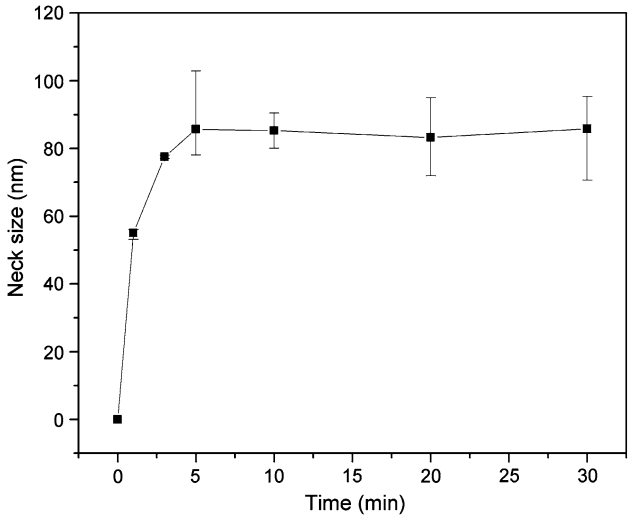

Fig. 7. Relation between neck size of silver NPs and sintering time at 200°C.

showed clear sintering and neck growth between silver NPs at 100°C and 150°C. No coalescence was observed at these low temperatures. As the sintering temperature increased to 200°C, coalescence and grain growth started to appear in some areas. Dramatic coalescence and grain growth to 500 nm was observed at 250°C and 300°C.

Metallurgical Bond between Copper and Silver NPs

To get a uniform distribution of silver NPs, multiple depositions of the NP paste onto the copper foil were performed. Figure 9a clearly shows the CRE after one deposition, i.e., there was high concentration of NPs in the ring and relatively less distribution in the central area. After multiple depositions, the CRE disappeared and more uniform thickness of the silver NPs was achieved, as shown in Fig. 9b.

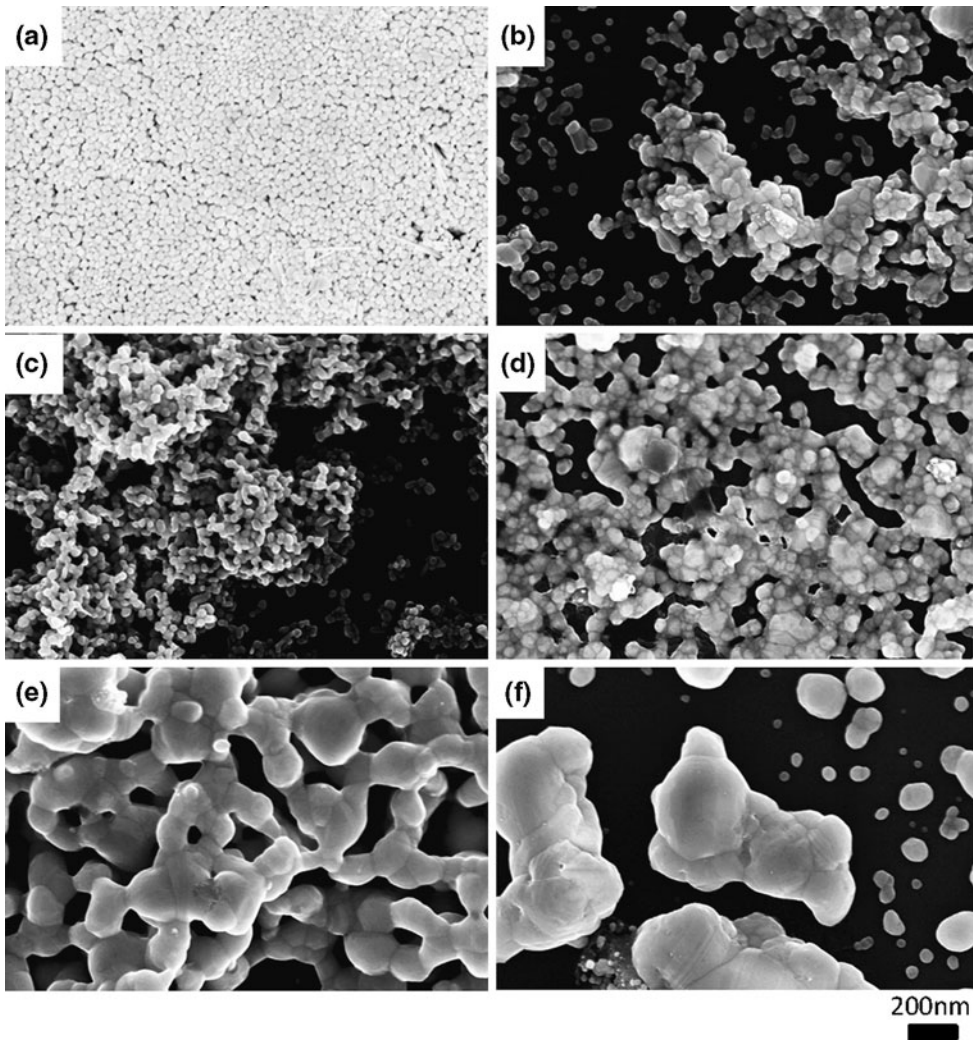

Fig. 8. SEM images of silver NPs (a) at RT and sintered for 30 min at (b) 100°C, (c) 150°C, (d) 200°C, (e) 250°C, and (f) 300°C.

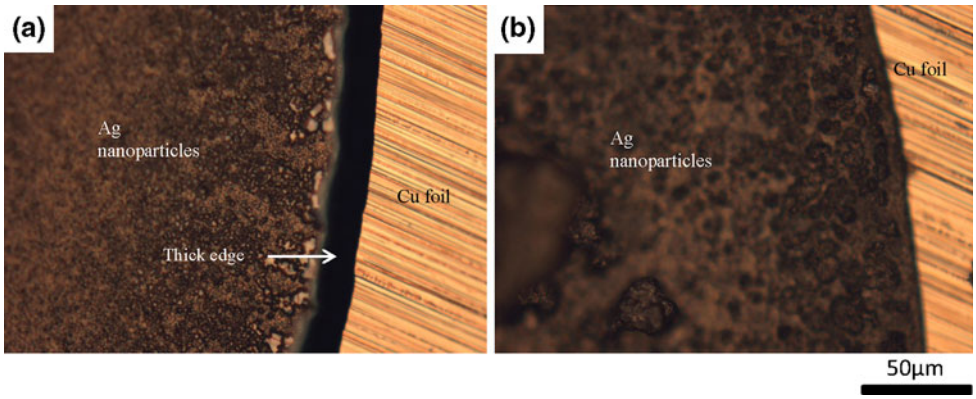

Fig. 9. Distribution control of silver NPs by (a) one deposition and (b) multiple depositions.

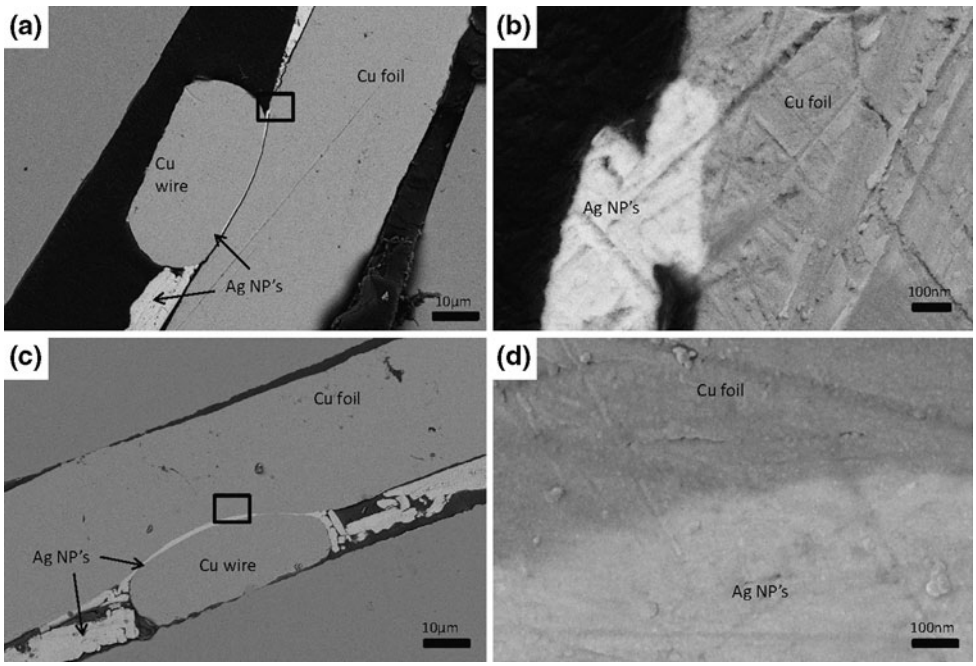

Fig. 10. Cross-sectional SEM images of copper wire bonded to copper foil (a) at 160°C, (b) higher magnification of (a), (c) at 200°C, and (d) higher magnification of (c).

Figure 10 shows cross-sectional SEM images of joints formed with 50-μm copper wires at 160°C and 200°C. The joint formed at 160°C showed close contact between the sintered silver NPs and the wire while there was a remarkable gap between the NPs and the foil except for a small area. The partial joining is not expected to provide a strength that can cause wire fracture, as will be discussed in the shear strength results. Thus, it is reasonable to deduce that some joined areas between copper foil and silver NPs broke during preparation of SEM samples. This gap also indicates that the wire–NPs joint was stronger than the foil–NPs joint. At 200°C, there was always close contact between the NPs and copper at both sides of the joint.

The SEM images of the bonded samples clearly showed the effect of pressure on the sintering behavior of the silver NPs compared with pressureless sintering in Figs. 6 and 8. Under pressure of 5 MPa, the porosity that was shown in the pressureless sintering disappeared and the NPs formed a bulk layer without distinguishable particle morphology. These images also show clear plastic deformation of the wire and the foil as a result of the 5 MPa applied pressure.

TEM images of the interfaces of a joint bonded at 250°C are shown in Fig. 11 between 50-μm copper wire and silver NPs, and in Fig. 12 between silver NPs and copper foil. Close contact at the lattice level between silver and copper is shown in Figs. 11b and 12b. High-resolution TEM images show that both copper wire and copper foil are nanocrystalline. This may have enhanced the diffusion process with the silver NPs. The dark areas on both sides of the

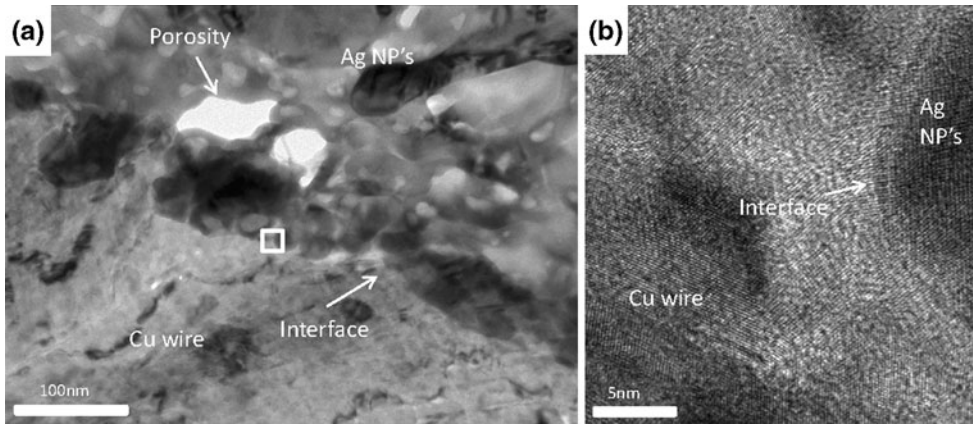

Fig. 11. TEM images of copper wire–silver interface (a) at low resolution and (b) at high resolution.

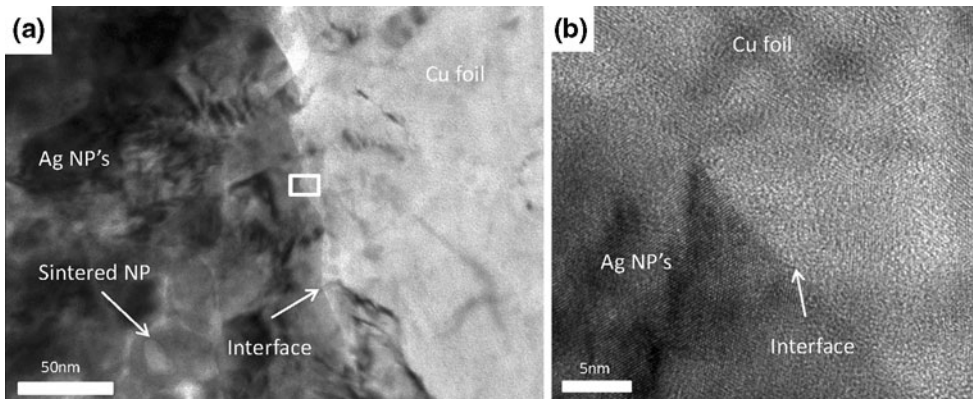

Fig. 12. TEM images of copper foil–silver interface (a) at low resolution and (b) at high resolution.

interface were caused by the nonuniform thickness of the TEM sample.

The previously reported microstructure analysis of the bonds formed by silver NPs showed a distorted layer of about 3 nm between lattices of silver and copper.[11–13] The presence of the distorted layer in the current work cannot be confirmed due to the nanocrystalline nature of the NPs, the foil, and the wire.

Shear Strength

The lowest temperature at which a bond could be formed was 160°C, which is the same temperature at which the organic shell decomposed. Table I presents the shear strength of the bonded samples for copper wires of three different diameters. All measurements were carried out at RT except one set of tests performed at 250°C for 250-μm wire bonded at 200°C. Shear tests of 50-μm copper wires resulted in the wire breaking for all bonding temperatures. Thus, under pure shear load, 160°C provides sufficient joint strength that the wire fractures before the joint. This is an even lower temperature than the lowest reported bonding temperature of 250°C.[11–13]

If the fracture occurs at the wire, the shear strength measured is actually the critical tensile strength of the wire, which is less than the real shear strength of the joint. To examine the real strength of the joints, 250-μm and 500-μm wires were tested. The 250-μm wire showed joint fracture at 200°C and wire fracture at 250°C. For 500-μm wire, joint fracture occurred at 200°C, 250°C, and 300°C, and the joint strength increased as the bonding temperature increased due to enhanced sintering of NPs at higher temperatures. This trend could not be observed with the 50-μm wire since the fracture occurred at the wire for all bonding temperatures.

For microelectronic application, 50-μm wire is more popular than 250-μm wire. Although the bonds formed below 250°C had very low shear strength values (Table I), they are strong enough to break the 50-μm wire. Besides, for thicker wire, higher bonding temperature is recommended. The reported shear strength values of joints formed by silver NPs were 27 MPa at 250°C[13] and 36 MPa at 300°C.[11] Although these shear strength values are higher than our values for the same bonding temperature, previous work on bonding below 250°C was unsuccessful.

Table I. Shear strength of the joints

Wire Diameter (μm)	Bonding Temperature (°C)	Average Shear Strength (MPa)	Coefficient of Variation	Fracture Type
50	140	0	0	Joint
50	160	2.8	0.26	Wire
50	200	3.2	0.38	Wire
50	250	2.5	0.17	Wire
250	200	4.2	0.13	Joint
250	200[a]	7.0	0.13	Wire
250	250	11.9	0.06	Wire
500	200	3.9	0.12	Joint
500	250	17.3	0.15	Joint
500	300	21.9	0.02	Joint

[a]Tested at 250°C

Shear tests were also performed at temperatures above the bonding temperatures to examine joint reliability at higher operating temperatures. Table I shows that a bond formed with 250-μm wire at 200°C had higher shear strength when tested at 250°C than when tested at RT. This clearly indicates that bonds formed by our method do not degrade at temperatures above the bonding temperature. The increase in strength might be due to enhanced sintering of silver NPs at higher test temperatures.

CONCLUSIONS

Copper wire and copper foil were successfully bonded together by solid-state sintering of silver NP paste at low temperatures down to 160°C. The silver NP paste was developed by increasing the concentration of 0.001 vol.% silver NP sol to 0.1 vol.% through centrifugation. Silver nitrate ($AgNO_3$) was reduced by sodium citrate dihydrate ($Na_3C_6H_5O_7 \cdot 2H_2O$) to fabricate the 0.001 vol.% sol. The silver NPs were coated with a citrate organic shell that decomposes at 160°C and promotes bonding with the copper. Under shear tests, bonds formed at 160°C and 250°C had enough strength to cause wire fracture for 50-μm and 250-μm wires, respectively. Shear tests of 500-μm wire showed that the strength of the bond increased as the bonding temperature increased due to enhanced sintering of silver NPs at higher temperature. Microstructure analysis of the joint cross-sectional area confirmed the metallic bond between the silver NPs and the copper. Bonds formed by sintering of silver NPs are proved to withstand temperatures above their bonding temperature.

ACKNOWLEDGEMENT

The authors acknowledge the financial support of NSERC discovery grants.

REFERENCES

1. Y. Zhou, eds., *Microjoining and Nanojoining* (Cambridge, UK: CRC/Woodhead, 2008).
2. Y. Zhou, A. Hu, M.I. Khan, W. Wu, B. Tam, and M. Yavuz, *J. Phys. Conf. Ser.* 165, 012021 (2009).
3. H. Tatsumi, Y. Akada, T. Yamaguchi, and A. Hirose, *Adv. Mater. Res.* 26–28, 499 (2007).
4. T. Morita, Y. Yasuda, E. Ide, Y. Akada, and A. Hirose, *Mater. Trans.* 49, 2875 (2008).
5. Z.Z. Fang and H. Wang, *Int. Mater. Rev.* 53, 326 (2008).
6. K. Moon, H. Dong, R. Maric, S. Pothukuchi, A. Hunt, Y. Li, and C.P. Wong, *J. Electron. Mater.* 34, 168 (2005).
7. M. Yeadon, J. Yang, R. Averback, J. Bullard, and J. Gibson, *Nanostruct. Mater.* 10, 731 (1998).
8. K.K. Nanda, A. Maisels, F.E. Kruis, H. Fissan, and S. Stappert, *Phys. Rev. Lett.* 91, 106102 (2003).
9. Q. Jiang, S.H. Zhang, and J.C. Li, *Solid State Commun.* 130, 581 (2004).
10. R. German, *Sintering Theory and Practice* (New York, John Wiley & Sons, Inc, 1996), p. 70.
11. E. Ide, A. Angata, A. Hirose, and K.F. Kobayashi, *Acta Mater.* 53, 2385 (2005).
12. Y. Akeda, H. Tatsumi, T. Yamaguchi, A. Hirose, T. Morita, and E. Ide, *Mater. Trans.* 49, 1537 (2008).
13. T. Morita, E. Ide, Y. Yasuda, A. Hirose, and K. Kobayashi, *Jpn. J. Appl. Phys.* 47, 6615 (2008).
14. E. Ide, S. Angata, A. Hirose, and K.F. Kobayashi, *Mater. Sci. Forum* 512, 383 (2006).
15. D. Wakuda, M. Hatamura, and K. Suganuma, *Chem. Phys. Lett.* 441, 305 (2007).
16. D. Wakuda, K. Kim, and K. Suganuma, *IEEE Trans. Compon. Packag. Technol.* 32, 627 (2009).
17. A. Hu, J.Y. Guo, H. Alarifi, G. Patane, Y. Zhou, G. Compagnini, and C.X. Xu, *Appl. Phys. Lett.* 97, 153117 (2010).
18. D.V. Goia and E. Matijević, *N. J. Chem.* 22, 1203 (1998).
19. P.C. Lee and D. Meisel, *J. Phys. Chem.* 86, 3391 (1982).
20. Y. Badr, M.G. Abd El Wahed, and M.A. Mahmoud, *Appl. Surf. Sci.* 253, 2502 (2006).
21. Y. Tan, Y. Li, and D. Zhu, *J. Colloid Interf. Sci.* 258, 244 (2003).
22. R. Deegan, *Phys. Rev. E* 61, 475 (2000).
23. H. Tada, J. Bronkema, and A.T. Bell, *Catal. Lett.* 92, 93 (2004).
24. E.L. Force and A.T. Bell, *J. Catal.* 38, 440 (1975).
25. L. Ding, R. Davidchack, and J. Pan, *Comput. Mater. Sci.* 45, 247 (2009).